Sudden expansion and domain-wall melting of strongly interacting bosons in two-dimensional optical lattices and on multileg ladders

Johannes Hauschild, Frank Pollmann, and Fabian Heidrich-Meisner

Phys. Rev. A **92**, 053629 — Published 30 November 2015

DOI: 10.1103/PhysRevA.92.053629

Sudden expansion and domain-wall melting of strongly interacting bosons in two dimensional optical lattices and on multi-leg ladders

Johannes Hauschild,[1] Frank Pollmann,[1] and Fabian Heidrich-Meisner[2]

[1] *Max Planck Institute for the Physics of Complex Systems, D-01187 Dresden, Germany*
[2] *Department of Physics and Arnold Sommerfeld Center for Theoretical Physics, Ludwig-Maximilians-Universität München, D-80333 München, Germany*

We numerically investigate the expansion of clouds of hard-core bosons in the two-dimensional square lattice using a matrix-product state based method. This nonequilibrium set-up is induced by quenching the trapping potential to zero and our work is specifically motivated by a recent experiment with interacting bosons in an optical lattice [Ronzheimer *et al.*, Phys. Rev. Lett. **110**, 205301 (2013)]. As the anisotropy of the amplitudes J_x and J_y for hopping in different spatial directions is varied from the one- to the two-dimensional case, we observe a crossover from a fast ballistic expansion in the one-dimensional limit $J_x \gg J_y$ to much slower dynamics in the isotropic two-dimensional limit $J_x = J_y$. We further study the dynamics on multi-leg ladders and long cylinders. For these geometries we compare the expansion of a cloud to the melting of a domain wall, which helps us to identify several different regimes of the expansion as a function of time. By studying the dependence of expansion velocities on both the anisotropy J_y/J_x and the number of legs, we observe that the expansion on two-leg ladders, while similar to the two-dimensional case, is slower than on wider ladders. We provide a qualitative explanation for this observation based on an analysis of the rung spectrum.

PACS numbers: 67.85.-d, 05.30.Jp, 37.10.Jk

I. INTRODUCTION

Ultracold quantum gases are famous for the possibility of realizing many-body Hamiltonians such as the Hubbard model, the tunability of interactions strengths and effectively, also dimensionality [1]. This provides access to genuine one-dimensional (1D) and two-dimensional (2D) physics as well as to the crossover physics between these limiting cases. Moreover, time-dependent changes of various model parameters can be used to explore the nonequilibrium dynamics of many-body systems (see [2–4] for recent reviews). Timely topics that are investigated in experiments include the relaxation and thermalization dynamics in quantum quenches [5–14], the realization of metastable states [15, 16], and nonequilibrium mass- [17–19] and spin transport [20]. Due to the availability of powerful analytical and numerical methods such as bosonization [21], exact solutions for integrable systems [22], or the density matrix renormalization group method [23–25], a direct comparison between theoretical and experimental results is often possible in the case of 1D systems [8, 10, 13, 19].

Strongly interacting many-body systems in two spatial dimensions, however, pose many of the open problems in condensed matter theory and many-body physics, concerning both equilibrium and nonequilibrium properties. The reason is related to the lack of reliable numerical approaches. Exact diagonalization, while supremely flexible, is inherently restricted to small system sizes [26]. Nevertheless, smart constructions of truncated basis sets by selecting only states from subspaces that are relevant for a given time-evolution problem have given access to a number of 2D nonequilibrium problems (see, e.g., [27, 28]). The truncation of equation of motions for operators provides an alternative approach [29], which has also been applied to quantum quench problems in the 2D Fermi-Hubbard model [30]. Quantum Monte Carlo methods can be applied to systems in arbitrary dimensions including nonequilibrium problems (see, e.g., [31–33]), but suffer, for certain systems and parameter ranges, from the sign problem [34]. Dynamical mean-field methods become accurate in higher dimensions, yet do not necessarily yield quantitatively correct results in 2D [35].

Regarding analytical approaches, we mention just a few examples, including solutions of the Boltzmann equation [17], flow equations [36], expansions in terms of the inverse coordination number [37], semiclassical approaches [38, 39], or time-dependent mean-field approaches [40–42] such as the time-dependent Gutzwiller ansatz (see, e.g., [43, 44]). All these methods have provided valuable insights into aspects of the nonequilibrium dynamics in two (or three) dimensions, yet often involve approximations. Recently, the application of a nonequilibrium Green's function approach to the dynamics in the sudden expansion in the 2D Fermi-Hubbard model has been explored [45].

Although there have been very impressive recent applications [46–48] of the density-matrix renormalization group (DMRG) method [23] to 2D systems, the method in general faces a disadvantageous scaling with system size in 2D [24, 48]. Tensor-network approaches [49–51] that were specifically designed to capture 2D many-body wave-functions are an exciting development, with promising results for the $t-J$ model [52]. A relatively little explored area of research is the time evolution of 2D many-body systems in quantum quench problems using DMRG type algorithms [53–57].

In this work, we present the application of a recent

extension [53] of 1D matrix-product state (MPS) algorithms [58–60] that is specifically tailored to deal with long-range interactions. Such long range interactions arise by mapping even a short-range Hamiltonian on a 2D lattice to a 1D chain for the application of DMRG.

Recent experiments have started to study the nonequilibrium dynamics of interacting quantum gases in 2D lattices or in the 1D-to-2D crossover [17, 19, 61]. Motivated by Refs. [16, 19], we study the sudden expansion of hard-core bosons which is the release of a trapped gas into a homogeneous optical lattice after quenching the trapping potential to zero. The results of Ref. [19] show that strongly interacting bosons in 2D exhibit a much slower expansion than their 1D counterpart. In the latter case, the integrability of HCBs leads to a strictly ballistic and (for the specific initial conditions of Ref. [19]) fast expansion that is indistinguishable from the one of non-interacting fermions and bosons. In the 2D case, it is believed that diffusive dynamics sets in and virtually inhibits the expansion in the high-density region, leading to a stable high-density core surrounded by ballistically expanding wings [19], similar to the behavior of interacting fermions in 2D [17]. The characteristic feature of these diffusive-like expansions in contrast to the ballistic case is the emergence of a spherically symmetric high-density core, while the ballistic expansion unveils the topology of the underlying reciprocal lattice.

In our work, we investigate this problem for both 2D clusters that can expand symmetrically in the x- and y-direction [see Fig. 1(a)] and wide cylinders and ladders [see Fig. 1(b)]. We use the ratio of hopping matrix elements J_x and J_y along the x- and y-direction as a parameter to study the 1D-to-2D crossover. For the 2D expansion in the isotropic case $J_x = J_y$, we clearly observe the emergence of a spherically symmetric core, while for small values of $J_y < J_x$ and on the accessible time scales, the expansion is essentially 1D like. We further compute the expansion velocities derived from the time dependence of the radius as a function of J_y/J_x.

Since we are in general able to reach both longer times and larger particle numbers in the case of ladders than in 2D, we present an extensive analysis of multi-leg ladders and cylinders (i.e., ladders with periodic boundary conditions in the (narrow) y-direction) with $L_y = 2, 3, 4$ legs [see the sketch in Fig. 1(b)]. From the analysis of the expansion in 1D systems [16], we expect that the short-time dynamics is identical to the melting of so-called domain-wall states [62–64], in which half of the system is empty while the other half contains one particle per site in the initial state [see the sketch in Fig. 1(c)]. The domain-wall melting has been attracting considerable attention as a nonequilibrium problem in 1D spin-1/2 systems (see, e.g., [62–69]). Our results show that this similarity between the expansion of clusters and the domain-wall melting carries over to the transient dynamics on L_y-leg ladder systems, irrespective of boundary conditions.

A considerable portion of the discussion in both theoretical and experimental papers has focussed on the question whether there are signatures of diffusive dynamics in the sudden expansion in 2D, in the dimensional crossover [17, 19] or on coupled chains [70]. The analysis of the expansion of fermions in the 2D square lattice starting from an initial state with two particles per site (i.e., a fermionic band insulator) suggests that diffusive dynamics is responsible for the slow expansion in the high-density regions [17]. This is expected to carry over to the bosonic case, yet there, only two-leg ladders have been thoroughly studied. In linear response, hard-core bosons on a two-leg ladder realize a textbook diffusive conductor at high temperatures [71, 72], thus suggesting that diffusion may also play a role in the sudden expansion [70]. Curiously, the expansion velocities measured numerically for hard-core bosons on a two-leg ladder exhibit a dependence on J_y/J_x that resembles the experimental observations for the true 2D case [19, 70]. Here, we are able to provide a more refined picture. Our analysis unveils that the sudden expansion becomes faster by going from two-leg to three- or four-leg ladders. We trace this back to the existence of heavy excitations on the two-leg ladder that are defined on a rung of the ladder and are inherited from the $J_x \ll J_y$ limit, which cannot propagate in first-order tunneling processes in J_x/J_y. Conversely, the three- and four-leg ladders possess single-particle like excitations, which we dub propagating modes, that have a sufficiently low mass to become propagating. This picture provides an intuitive understanding of the emergence of slow mass transport in the sudden expansion in the initial stages of the time evolution, complementary to the discussion of diffusive versus ballistic dynamics. The reasoning is similar to the role that doublons play for slowing down mass transport in the 1D Bose-Hubbard model [19, 70, 73–75], which has also been emphasized in the case of the Fermi-Hubbard model [76, 77]. Our results raise the question whether the expansion in both directions in 2D and the one-directional expansion on wide ladders and cylinders will result in the same dependence of expansion velocities on J_y/J_x for large L_y. It appears that the ladders and cylinders, at least for small L_y, preserve some degree of one-dimensionality. A possible scenario is that the expansion velocities in the x-direction will depend non-monotonically on L_y for a fixed value of J_y/J_x if ever they will become identical to the behavior on the

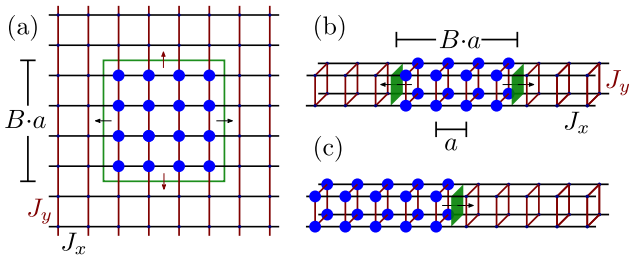

FIG. 1. Illustration of initial states and geometries: (a) central block for the 2D expansion; (b) central block of size $B \times L_y$ and (c) domain wall on a cylinder with $L_y = 4$ legs.

2D systems. As a caution, we stress that long expansion times may be necessary to fully probe the effect of a 2D expansion at small $J_y \ll J_x$ since the bare time scale for charge dynamics in the y-direction is set by $1/J_y$, as has been pointed out in [78].

Apart from the nonequilibrium mass transport of strongly interacting bosons, there are also predictions for the emergence of nonequilibrium condensates at finite quasimomenta in the sudden expansion in a 2D square lattice. These predictions are based on exact diagonalization for narrow stripes [79] as well as on the time-dependent Gutzwiller method [43, 44]. The dynamical condensation phenomenon has first been discussed for 1D systems (where it actually is a quasicondensation [80]), where it was firmly established from exact numerical results [80, 81] and analytical solutions [64] (see also [70, 82–84]) and has recently been observed in an experiment [16]. In the sudden expansion of hard-core bosons in one dimension, the dynamical quasicondensation is a transient, yet long-lived phenomenon [70, 80] as ultimately the quasimomentum distribution function of the physical particles approaches the one of the underlying noninteracting fermions via the dynamical fermionization mechanism [85, 86].

It is therefore an exciting question whether a true nonequilibrium condensate can be generated in 2D. Our results cannot fully clarify this point, yet we do observe a bunching of particles at certain non-zero momenta in the quasimomentum distribution after releasing the particles whenever propagating modes as discussed above are present. For the melting of domain walls, the occupation of most of these modes, at which a nonequilibrium condensation is allowed by energy conservation and at which a bunching occurs, saturates at long expansion times. The notable exception are certain modes on the $L_y = 4$ cylinder. This behavior, i.e., the saturation is markedly different from the 1D case of hard-core bosons in the domain-wall melting, where the occupation continuously increases. The reason for this increase is that the semi-infinite, initially filled half of the system will indefinitely feed the quasicondensates [16, 64]. As such an increase is a necessary condition for condensation, we interpret the saturation of occupations as an indication that either breaking the integrability of strictly 1D hard-core bosons or the larger phase space for scattering in 2D inhibits the dynamical condensation of expanding clouds. However, even in those cases on the ladder, in which we do not see a saturation, the increase is slower than the true 1D case, suggesting that coupling chains in general disfavors condensation. Yet, a decisive analysis of this problem will require access to larger particle numbers and times in numerical simulations or future experiments. Note that multi-leg ladder systems can be readily realized with optical lattices, using either super-lattices [87] or the more recent approach of using a synthetic lattice dimension [88–90].

The plan of this paper is the following. In Sec. II, we introduce the model and definitions. Section III provides a discussion and definitions for various measures of expansion velocities employed throughout our work, while Sec. IV provides details on our numerical method. We present our results for the 2D case in Sec. V, while the results for multi-leg ladders and cylinders are contained in Sec. VI. We conclude with a summary presented in Sec. VII, while details on the extraction of velocities and on the diagonalization of rung Hilbert spaces are contained in two appendices.

II. MODEL AND INITIAL CONDITIONS

We consider hard-core bosons on a square lattice and on multi-leg ladders. The Hamiltonian reads

$$H = -\sum_{i_x,i_y} [J_x(\hat{a}^\dagger_{i_x,i_y}\hat{a}_{i_x+1,i_y} + h.c.) + J_y(\hat{a}^\dagger_{i_x,i_y}\hat{a}_{i_x,i_y+1} + h.c.)] . \quad (1)$$

Here, $\hat{a}^\dagger_{i_x,i_y}$ denotes the creation operator on site $\mathbf{i} = (i_x, i_y)$ and $J_x(J_y)$ are the hopping matrix elements in $x(y)$ direction. We choose the hopping matrix element J_x in x-direction and the lattice constant a as units and set $\hbar$ to unity; the ratio J_y/J_x is dimensionless. Note that the Hamiltonian is equivalent to the spin-1/2 XX-model. In 1D ($J_y = 0$), the Jordan-Wigner transformation maps the bosons to free fermions [91]. L_x and L_y denote the number of sites in the x- and y-direction, respectively.

We consider different geometries, namely (i) a small square-shaped cluster of $L_x = L_y = 12$ sites with open boundary conditions in both directions, (ii) ladders with $L_x = 60$, $L_y \in \{2, 3, 4\}$ with open boundary conditions (OBC) in both the x- and y-direction, and (iii) cylinders with $L_x = 60$, $L_y \in \{2, 3, 4\}$ with periodic boundary conditions (PBC) in y-direction and open boundary conditions in x-direction. For two-leg ladders, the only difference between the Hamiltonian with OPC and PBC along the y-direction is thus a factor of two in the tunneling matrix element J_y. In praxis, we obtain the behavior with PBC by just taking the OBC data with $J_y \to J_y/2$.

For all simulations, we start the expansion from a product state

$$|\psi_0\rangle = \prod_{\mathbf{i}\in\mathcal{B}} \hat{a}^\dagger_{i_x,i_y} |\text{vac}\rangle \quad (2)$$

in real space. To model the fully 2D expansion, we choose $\mathcal{B}$ to be a square-shaped block of $B \times B$ sites centered in the cluster, see Fig. 1(a). On cylinders and ladders, we study two different types of $\mathcal{B}$: (i) a block of $B \times L_y$ bosons, centered in x-direction and filling all the sites in y-direction as shown in Fig. 1(b), and (ii) a domain wall, where the left half of the lattice is occupied by a block of $L_x/2 \times L_y$ bosons while the right half is empty, see Fig. 1(c).

III. DEFINITIONS OF EXPANSION VELOCITIES

There are several possible ways of defining the spatial extension of an expanding cloud, and thus also several different velocities.

A. Position of the fastest wavefront

One can define the cloud size from its maximum extension, i.e., from the position of the (fastest) wavefront. The velocity derived from this approach will typically simply be the fastest possible group velocity (provided the corresponding quasimomentum is occupied in the initial state). Thus, this velocity will not contain information about the slower moving particles and any emergent slow and possibly diffusive dynamics in the core region. We do not study the wavefront in this work.

B. Radial velocity

Theoretically, it is natural to define the radius R as the square root of the second moment of the particle distribution $\langle n_i(t)\rangle$. Supposed we are interested in the expansion in x-direction, we average the density profile over the y-direction to calculate the radius

$$R_x^2(t) = \frac{1}{N}\sum_{i_x,i_y} n_{i_x,i_y}(t)(i_x a - i_x^0 a)^2, \tag{3}$$

where $i_x^0 a$ is the center of mass in x-direction and N is the total number of bosons. An analogous expression is used to define R_y^2. To get rid of an initial constant part, we use $\tilde{R}_\mu^2(t) = R_\mu^2(t) - R_\mu^2(t=0)$ to define the radial velocity

$$v_{r,\mu} = \frac{\partial \tilde{R}_\mu(t)}{\partial t} \tag{4}$$

with $\mu = x, y$. The corresponding velocity has contributions from all occupied quasimomenta. It will ultimately be dominated by the fastest expanding particles, and for the sudden expansion, R will be linear in time in the limit in which the gas has become dilute and effectively noninteracting.

The radial expansion velocity of 1D systems was studied for the Fermi-Hubbard model [92], the Bose-Hubbard model [19, 70], and the Lieb-Liniger model [93]. For Bethe-integrable 1D systems, it can be related to distributions of rapidities [94]. For a recent study of the radial velocity in the 2D Fermi-Hubbard model, see [45].

C. Core expansion velocity

In the related experiments with ultracold atoms [17, 19], the focus was on the core expansion velocity that is derived from the time evolution of the half-width-at-half maximum $r_c(t)$. The reason is primarily that in these experiments, an average over many 1D or 2D systems is measured. Moreover, the core expansion velocity is primarily sensitive to the dynamics in the high-density core (but insensitive to the ballistic tails) and thus yields slightly different information. In case of multiple local maxima, the two outermost points are taken. Since in our simulations we have smaller particle numbers compared to the experiments [17, 19], we use linear splines to interpolate the density profile between the lattice sites in order to get values for $r_c(t)$ to a better accuracy than just a single lattice constant. The core expansion velocity is defined as the time derivative

$$v_c = \frac{\partial r_c(t)}{\partial t}\,. \tag{5}$$

The full time dependence of r_c and the extraction of v_c is discussed in Appendix A.

IV. NUMERICAL METHOD

Although the Hamiltonian Eq. (1) itself is short ranged, long-range interactions arise by mapping the 2D lattice to a 1D DMRG-chain. The presence of such long-range interactions renders most of the existing DMRG based algorithms for the time evolution [25, 58–60] inefficient because a direct Trotter decomposition of the exponential is not possible. In our work, we use a recently developed extension of an MPS based time-dependent DMRG algorithm that is particularly suited for such systems [53]. The method is based on a local version of a Runge-Kutta step which can be efficiently represented by a matrix-product operator (MPO) [95]. The actual time evolution can then be performed using standard alorithms that apply an MPO to a given MPS [25]. An advantage of the method is that it can be easily implemented into an existing MPS based DMRG code and has a constant error per site.

For our simulations, we choose the DMRG-chain to wind along the y-direction in order to keep the range of the interactions as small as possible (namely L_y). Sources of errors are the discretization in time and the discarded weight per truncation of the MPSs after each time step. The time steps are chosen small enough to make the error resulting from the second order expansion negligible. We furthermore choose the truncation error at each step to be smaller than 10^{-10} which is sufficient to obtain all measured observables accurately. The growth of the entanglement entropy following the quench requires to increase the bond dimension χ with time. Conversely, since we restrict the number of states to $\chi \lesssim 2000$, we are naturally limited to a finite maximum time t_m at which the truncation error becomes significant. Note that the bond dimension χ required for the simulations grows exponentially with time. Increasing the particle numbers and L_y leads to a faster growth of the entanglement entropy

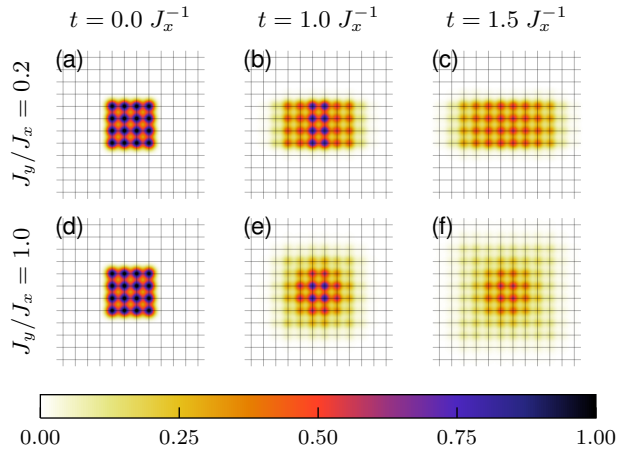

FIG. 2. (Color online) Density profiles for the 2D expansion from a 4×4 cluster with (a)-(c) $J_y/J_x = 0.2$ and (d)-(f) $J_y/J_x = 1.0$ at times $tJ_x = 0.0, 1.0, 1.5$.

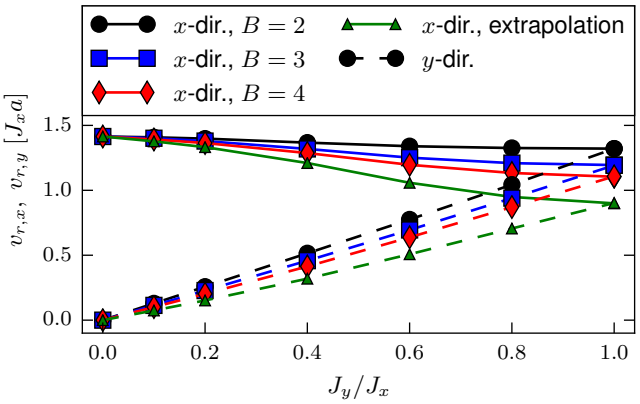

FIG. 3. (Color online) Radial velocity $v_{r,x/y}$ in x-direction (top three solid lines) and y-direction (dashed lines) for the 2D expansion from $B \times B$ clusters. The small green triangles show the result of an extrapolation to $B = \infty$ using Eq. (6).

and thus to a shorter maximal time t_m. However, we stress that we clearly reach longer times and larger systems than what is accessible with exact diagonalization (i.e., pure state propagation using, e.g., Krylov subspace methods).

V. TWO-DIMENSIONAL EXPANSION

A. Density profiles

We first characterize the expansion by analyzing the time- and position-resolved density profile $n_{i_x,i_y}(t) = \langle \hat{n}_{i_x,i_y}(t) \rangle$, where $\hat{n}_{i_x,i_y} = \hat{a}^\dagger_{i_x,i_y} \hat{a}_{i_x,i_y}$ is the number operator. We present exemplary density profiles for three different times and and two anisotropies $J_y/J_x \in \{ 0.2, 1 \}$ in Fig. 2. For small $J_y/J_x = 0.2$ [Figs. 2(a)-(c)], there is a fast expansion in x-direction and nearly no expansion in y-direction. This is expected since the bare timescale for the expansion in y-direction set by $1/J_y$ is here much larger than the one in x-direction [78]. On the other hand, for $J_y = J_x$, we find four "beams" of faster expanding particles going out along the diagonals. These beams are even more pronounced for initial states with smaller clusters of 2×2 and 3×3 bosons (not shown here).

The most important qualitative difference between the density profiles at $J_y/J_x = 0.2$ and $J_y/J_x = 1$ is the *shape*. In the former case, the profiles retain a rectangular form, reflecting the underlying reciprocal lattice and the different bare tunneling times in the x- versus y- direction. For the isotropic case, the initial square shape of the cluster changes into a spherically symmetrical form in the high-density region. This observation is consistent with the experimental results of [19].

B. Radial velocity

In order to compare the expansion for different values of J_y/J_x more quantitatively, we extract certain integrated quantities from the profiles, which contain relevant information. One such quantity is the radial velocity $v_{r,x/y}$ derived from the reduced radius $\tilde{R}_{x/y}$ [see Eq. (3)]. Details on how we extract v_r from the time-dependent reduced radius $\tilde{R}(t)$ can be found in Appendix A.

The radial velocities $v_{r,x}$ and $v_{r,y}$ for the 2D expansion are shown in Fig. 3. Unfortunately, our simulations for the 2D lattice are restricted to both very short times and small numbers of bosons with block sizes $B \in \{ 2, 3, 4 \}$. For instance, for 4×4 bosons we reach only times $t_m \approx 1.5\, J_x^{-1}$. The short times prevent us from a reliable extraction of the core expansion velocity, which would allow for a direct comparison to the experiment [17, 19]. The experimental results [19] suggest that for increasing J_y, the core expansion velocity in x-direction decreases dramatically [see Fig. 8], which has been attributed to the breaking of integrability of 1D hard-core bosons [19, 70].

Our results for the radial velocity v_r show that for the smallest block size $B = 2$, tuning J_y/J_x from 0 to 1 changes the velocity $v_{r,x}$ only gradually while the velocity in y-direction scales almost linearly with J_y. A previous study of the expansion of two-leg ladders also indicated that the core expansion velocity exhibits a much stronger dependence on J_y/J_x than the radial expansion velocity [70]. We suspect that this weak dependence may additionally result from the small number of bosons considered in our simulations: Increasing J_y allows a hopping in y-direction, which reduces the density and thus the effective interaction. In other words, tuning J_y/J_x from 0 to 1 increases the effective surface of the initial block to include the upper and lower boundary. From the surface, there is always a fraction of the bosons that escape and which effectively do not experience the hard-core in-

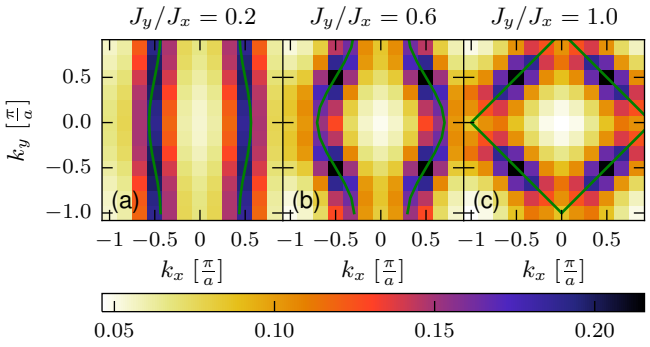

FIG. 4. (Color online) Momentum distribution function n_{k_x,k_y} [dimensionless] for the 2D expanding cloud of 4×4 bosons at time $t = 1.5\, J_x^{-1}$. The solid green lines show the solutions to Eq. (8).

teraction. This effect becomes more relevant for smaller boson numbers, where the bosons are almost immediately dilute, feel no effective interaction and thus expand (nearly) ballistically in both directions. For larger block sizes $B = 3, 4$, the ratio of surface to bulk is smaller and therefore, interaction effects become more relevant. Indeed, we find for $B = 3, 4$ that tuning J_y/J_x from 0 to 1 leads to a significant reduction of $v_{r,x}$, most pronounced for $B = 4$.

Even though we have access to only three values of B, it is noteworthy that for all values of J_y/J_x, $v_{r,x}(v_{r,y})$ decreases(increases) monotonically with B and thus with total particle number. This tendency is compatible with the behavior of the experiments [19] performed with much larger boson numbers, which motivates us to perform an extrapolation to $B = \infty$ despite the small number of bosons. We assume that the finite-size dependence is dominated by the surface effects of the initial boundary, which scales with B. Therefore, we extract the velocity for $B = \infty$ from a fit to the form

$$v_{r,x/y}(B) = v_{r,x/y}(B = \infty) + \frac{\text{const}}{B} \tag{6}$$

at fixed J_y/J_x. The resulting values, which are indicated by the small green symbols in Fig. 3, should only be considered as rough estimates.

C. Momentum distribution function

Figure 4 shows the momentum distribution function

$$n_{k_x,k_y} = \frac{1}{L_x L_y} \sum_{i_x,i_y,j_x,j_y} e^{-\mathrm{i}(k_x(i_x a - j_x a) + k_y(i_y a - j_y a))} \times \langle \hat{a}^\dagger_{i_x,i_y} \hat{a}_{j_x,j_y} \rangle \tag{7}$$

for the 2D expansion. For a purely 1D expansion ($J_y = 0$), dynamical quasicondensation occurs at $k_x = \pm\frac{\pi}{2a}$ [16, 80, 81]. As discussed in Refs. [43, 79], energy conservation restricts the (quasi)condensation to momenta at which the single-particle dispersion relation $\epsilon(k_x, k_y)$ vanishes since the initial state has zero energy, resulting in the emission of bosons with, on average, zero energy per particle. For a 2D system, this leads to

$$\epsilon(k_x, k_y) = -2J_x \cos(k_x a) - 2J_y \cos(k_y a) = 0. \tag{8}$$

The solutions of this equation are indicated by the solid green lines in Fig. 4. We indeed observe an accumulation of particles at momenta compatible with Eq. (8). For $J_y/J_x = 0.2$ [Fig. 4(a)], there is almost the same weight at any momentum k_y compatible with Eq. (8). We suspect that this is a relict of the short time $t = 1.5\, J_x^{-1} = 0.3\, J_y^{-1}$ reached in the simulations: up to this time there was almost no expansion in y-direction, thus we have roughly $\langle \hat{a}^\dagger_{i_x,i_y} \hat{a}_{j_x,j_y} \rangle \approx \delta_{i_y,j_y}$ such that n_{k_x,k_y} is initially independent of k_y. Nevertheless, closer inspection shows slightly more weight at compatible momenta with $k_y = \pm\frac{\pi}{2a}$ than at those with $k_y = 0$ even for small J_y [see Fig. 4(a)]. This becomes much more pronounced for $J_y = J_x$ [see Fig. 4(c)]. In this case, the strongest peaks are at $(k_x, k_y) = (\pm\frac{\pi}{2a}, \pm\frac{\pi}{2a}), (\pm\frac{\pi}{2a}, \mp\frac{\pi}{2a})$. These four points correspond to the maximum group velocities $v(k_x, k_y) = (2J_x a \sin(k_x a), 2J_y a \sin(k_y a))$ and, in real space, manifest themselves via the four "beams" in the density profile shown in Fig. 2(f).

Our results do not serve to clarify whether there actually is a dynamical condensation at finite momenta in 2D or not since our initial clusters have too few particles in the bulk compared to their surface. The fast ballistic propagation of the particles melting away from the surface will only be suppressed once the majority of particles is in the bulk initially. If we attribute the outermost particles to the surface, this would require us to be able to simulate at least 7×7 clusters. We believe that the accumulation at finite momenta seen in the quasimomentum distribution function is due to these fast particles melting away from the boundary during the first tunneling time. Moreover, we would need to be able to study the particle-number dependence of the height of the maxima in the quasimomentum distribution function or the decay of single-particle correlations over sufficiently long distances [80].

VI. CYLINDERS AND LADDERS

In contrast to the 2D lattice, the ratio of surface to bulk is much lower for cylinders and ladders, as we initialize the system uniformly in the y-direction. Moreover, if we tune J_y from 0 to 1, the additional hopping in the y-direction does not lower the density (and with it the effective interaction), as it is the case for the fully 2D expansion. We thus expect a weaker dependence of the results on the number of bosons. Additionally, we can reach larger times than for the fully 2D expansion since

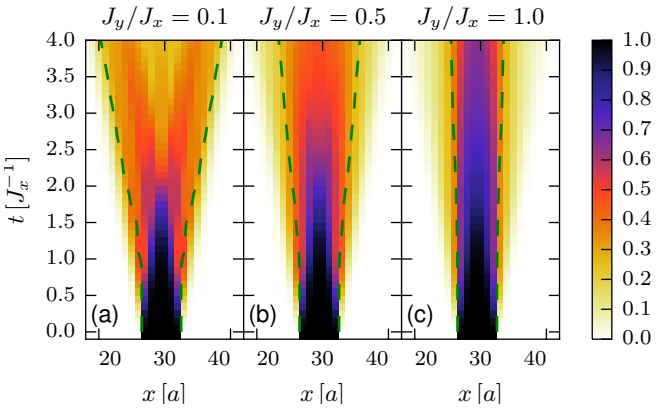

FIG. 5. (Color online) Integrated density profiles $\frac{1}{L_y}\sum_{i_y} n_{i_x,i_y}(t)$ [dimensionless] for the expansion from a 6×3 cluster on a cylinder with $L_y = 3$. The green dashed line shows the location of the half maximum on the left and right.

the range of hopping terms after mapping to the DMRG chain is smaller. While we can reach times up to $t_m \approx 6\,J_x^{-1}$ for $L_y = 2$, we are restricted to times up to $t_m \approx 4\,J_x^{-1}$ for $L_y = 3$ and $t_m \approx 3\,J_x^{-1}$ for $L_y = 4$.

A. Density profile

Figure 5 shows some typical results for the column density for the expansion of a block on a cylinder with $L_y = 3$. We identify three different time regimes for the expansion of blocks, schematically depicted in Fig. 6. First, the evolution during the first tunneling time $t_1 \propto 1/J_x$ is independent of J_y: Since we initialize our system uniformly in y-direction, in the initial longitudinal hopping, there cannot be any dependence on J_y and a finite amount of time is required before correlations in the y-direction can build up.

Then, in a transient regime $0 < t_2$ (where $t_2 > t_1$), the melting of the block from either side is equivalent to the domain-wall melting [16, 96] (compare the sketch in Fig. 1). From the two boundaries, two "light cones" emerge, consisting of particles outside and holes inside the block. Both particles and holes have a maximum speed of $v_m = 2\,J_x a$. Consequently, the time $t_2 := B/4J_x$ is the earliest possible time at which the melting arrives at the center, such that the density drops below one on all sites. Thus, t_2 marks the point in time at which density profiles obtained from blocks start to differ quantitatively from those of domain walls, defining the third time regime. In the case of a ballistic expansion realized for $J_y \ll J_x$, the density in the center drops strongly at t_2 and we can clearly identify two outgoing "jets" as two separating maxima in the density profiles, see Fig. 5(a). To be clear, the expectation for the nature of mass transport in a nonintegrable model such as coupled systems of 1D hard-core bosons is diffusion, based on numerical studies [71]. However, in the sudden expansion, the whole

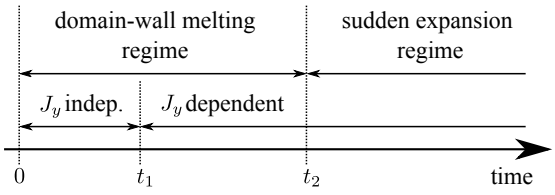

FIG. 6. Illustration of the time regimes for the expansion of blocks (see the text in Sec. VI A for details).

cloud expands and it is conceivable that the expansion appears to be ballistic because the cloud becomes dilute too fast, resulting in mean-free paths being in the order of or larger than the cloud size at any time [70].

On the other hand, for larger J_y the block in the center does not split at t_2, but a region with a high density ("core") remains in the center. The high-density core is clearly established already at intermediate $J_y/J_x = 0.5$, where it still expands slowly. For larger J_y, the spreading of this core is continuously suppressed.

B. Integrated current

In order to investigate the different time regimes further, we consider the number of bosons $\Delta N(t)$ that at a time t have left the block $\mathcal{B}$ where they were initialized. This is equivalent to the particle current $j^x_{i_x} = \mathrm{i}J_x \sum_{i_y}\langle \hat{a}^\dagger_{i_x+1,i_y}\hat{a}_{i_x,i_y} - \hat{a}^\dagger_{i_x,i_y}\hat{a}_{i_x+1,i_y}\rangle$ integrated over time and along the boundary $\partial\mathcal{B}$ of the block,

$$\Delta N(t) = \sum_{i\notin\mathcal{B}} n_{i_x,i_y}(t) = \int_0^t \mathrm{d}s\, \left[j^x_{b_r}(s) - j^x_{b_l}(s)\right]. \quad (9)$$

Here, b_r and b_l denote the right and left indices i_x of the boundary of the initially centered block $\mathcal{B}$. We compare ΔN for the expansion on a two-leg ladder starting from either central blocks or domain walls in Fig. 7(a). To this end we normalize ΔN by the boundary length $|\partial\mathcal{B}|$, which is simply $2L_y\,a$ for the central blocks and $L_y\,a$ for the domain walls.

For short times $t \lesssim 0.5\,J_x^{-1}$ (i.e., $t \lesssim t_1$, see the above), all curves in Fig. 7 are independent of J_y. For the quantity ΔN, the first deviations between domain walls and cylinders do not occur at t_2 but at $2t_2 = B/2J_x$, which is exactly the time the fastest holes need to travel once completely through the block: by definition, ΔN is not sensitive to the density inside the initial block. For the expansion of central blocks, particle conservation gives a strict bound $\Delta N/|\partial\mathcal{B}| \le B/2a$, in which case all the bosons have left the initial block. These bounds [equal to $1.5\,a^{-1}$ and $3\,a^{-1}$ for $B = 3$ and $B = 6$, respectively] are approached in the long-time limit of the ballistic expansion for small $J_y/J_x = 0.2$, which for $B = 6$, however, happens beyond the times reached in our simulations. For the domain walls, ΔN is not bounded (as long as the melting does not reach the boundary of the system) and

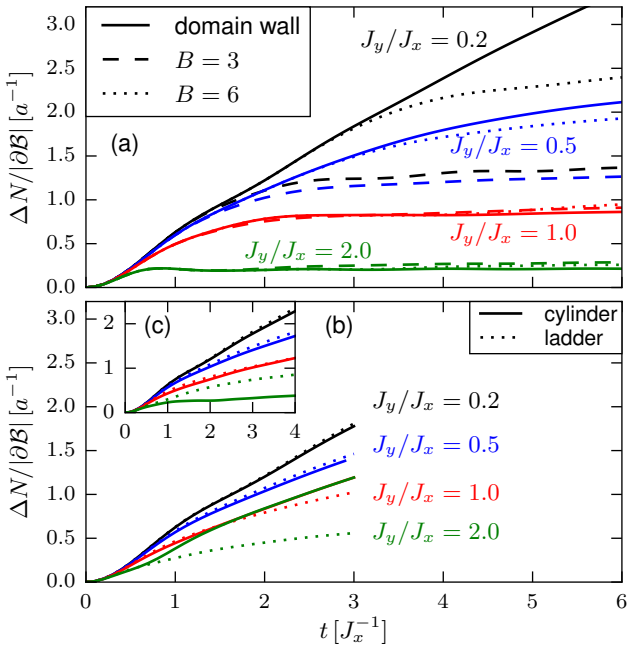

FIG. 7. (Color online) Comparison of $\Delta N/|\partial\mathcal{B}|$ (a) on a two-leg ladder for the expansion from central blocks (dashed/dotted lines, $B \times 2$ bosons) versus the melting of a domain wall (solid lines). The lower panels compare domain walls on ladders (dashed lines) to domain walls on cylinders (solid lines) for (b) $L_y = 4$ and (c) $L_y = 3$. The curves for the $L_y = 4$ cylinder in (b) with $J_y/J_x = 1, 2$ are nearly on top of each other for $t \gtrsim 1.5\, J_x^{-1}$.

grows for small J_y/J_x as $\Delta N \propto t$ linearly in time, which, via Eq. (9), corresponds to a non-decaying current j^x. On the other hand, ΔN gets almost constant for large J_y/J_x for both the domain walls and the blocks. This indicates that the expansion is strongly suppressed on the two-leg ladder, with a high-density core remaining in the center. We speculate that the regime in which ΔN increases only very slowly is indicative of diffusive dynamics, by similarity with [17].

C. Propagating modes: Limit of large $J_y \gg J_x$

In order to qualitatively understand the suppression of the expansion for certain geometries and specific values of L_y, it is very instructive to consider the limit of large $J_y \gg J_x$. We discuss this limit in more detail in Appendix B, while here, we provide only the general idea and discuss the results. The Hamiltonian Eq. (1) can be split up into the hopping on rungs [we denote sites with the same index i_x as a "rung" for both ladders and cylinders], denoted by H^y proportional to J_y, and the hopping terms in x-direction proportional to J_x, collected in H^x. Our analysis is based on a diagonalization of H^y, which is a block-diagonal product of terms operating on single rungs. We view the eigenstates of single rungs as "modes", which can be delocalized by H^x. Since a coherent movement of multiple bosons is a higher-order process of H^x and thus generally suppressed for large J_y/J_x, we focus on modes with a single particle on a rung. We then look for modes which are candidates for a propagation at finite k_x. Importantly, the kinetic energy $E_x \propto J_x$ cannot compensate for a finite $E_y \propto J_y$ for $J_y \gg J_x$. Since we initialize the system in states with zero total energy, energy conservation allows only modes with $E_y = 0$ to contribute to the expansion in first-order processes in J_x/J_y in time. In general, one could also imagine to create pairs of two separate bosons with exactly opposite E_y, summing up to 0. Yet, H^x cannot create such pairs [see Appendix B for details].

For smaller J_y, the scaling argument of the energy conservation does not hold and additional modes (beginning with those of small energy E_y) can be used for the propagation in x-direction – ultimately, for $J_y \ll J_x$ any mode contributes to the expansion already at short times. We note that modes with strictly $E_y = 0$ are either present or absent at any value of J_y/J_x.

Such propagating single-boson modes with $E_y = 0$ do *not* exist on a two-leg ladder: there are, apart from the empty and filled rung, only two states with large energies $E_y = \pm J_y$. We argue that precisely this lack of modes with $E_y = 0$ leads to the suppression of the expansion with increasing J_y/J_x. It is manifest in Fig. 7(a) by the fact that ΔN gets almost constant. Thus, we can view the expansion to be inhibited by the existence of heavy objects (particles of a large effective mass) that can propagate only via higher-order processes. This is similar to the reduction of expansion velocities due to doublons in the strongly interacting regime of the 1D Bose-Hubbard model [15, 19, 70, 74, 75]. Another effect with very similar physics is self-trapping (see, e.g., [44, 97, 98]).

Whether propagating modes with $E_y = 0$ exist or not depends not only on L_y but also on the boundary conditions in the y-direction. This can serve as a test for our reasoning. For $L_y = 4$, we find modes with $E_y = 0$ on a cylinder but not on a ladder (see Appendix B). We compare ΔN for these two geometries directly in Figs. 7(b) and (c). For small $J_y/J_x = 0.2$, the additional coupling of the cylinders compared to the ladders has (at least on the timescales accessible to us) nearly no influence. Yet, for large J_y/J_x, we find not only a quantitative but even a qualitative difference: For the $L_y = 4$ cylinders, ΔN increases linearly in time, irrespective of how large J_y/J_x is. Moreover, the slope is (at $t \gtrsim 1.5\, J_x^{-1}$) roughly the same for all $J_y/J_x \gtrsim 0.5$ and does almost not decrease with time. Using Eq. (9), we can relate this to the presence of a non-decaying current, which we explain in terms of an enhanced occupation at momenta compatible with $E_y = 0$. In contrast, on the four-leg ladder there are no propagating modes with $E_y = 0$, thus we expect no linear increase of ΔN. Indeed, we find that the currents – i.e., the slopes of ΔN in Fig. 7(c) – on the four-leg ladder decay in time. Yet, the decay is not as extreme as for

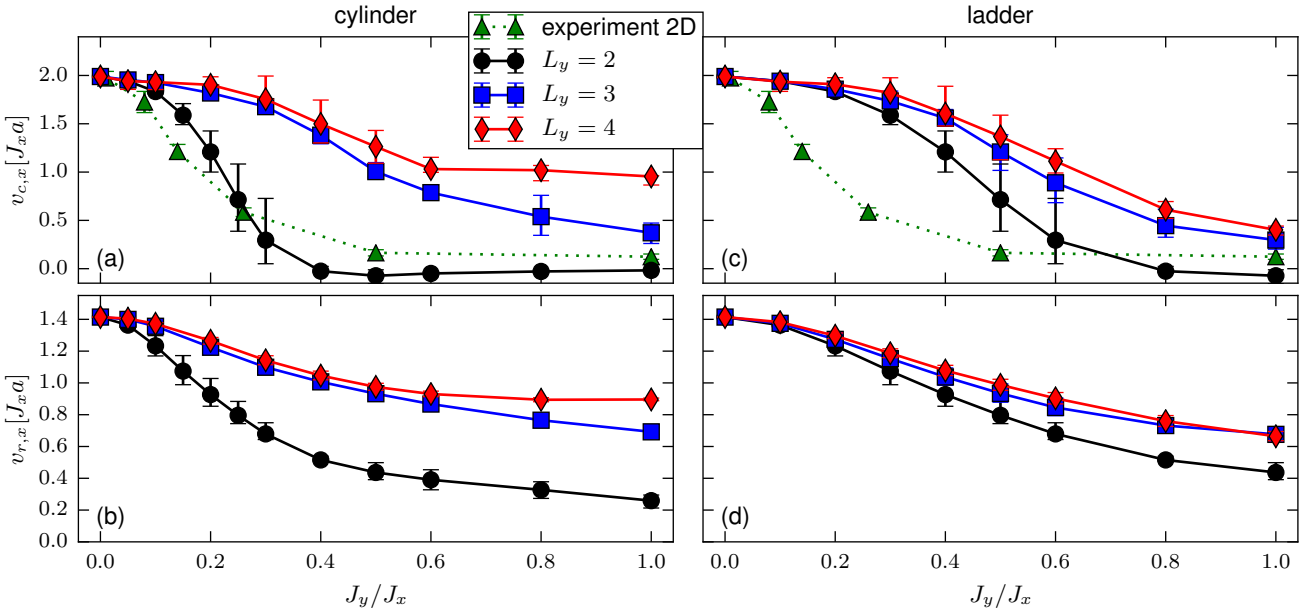

FIG. 8. (Color online) (a),(c) Core expansion velocities $v_{c,x}$ and (b),(d) radial velocities $v_{r,x}$ versus J_y for the expansion of a $6 \times L_y$ block. The left panels (a) and (b) are obtained on $L_y = 2, 3, 4$ cylinders, the right panels (c),(d) on $L_y = 2, 3, 4$ ladders. The green triangles taken from Ref. [19] show the results of the experiments for the fully 2D expansion corresponding to the setup of Sec. V.

the two-leg ladder, which we explain by the existence of modes with lower energies $E_y > 0$ than on the two-leg ladder. For $L_y = 3$, it is exactly the other way around: there are modes with $E_y = 0$ on the ladder but not on the cylinder. In agreement with this, Fig. 7(c) shows that the expansion on a three-leg ladder is faster than on an $L_y = 3$ cylinder for large $J_y/J_x = 2$.

D. Expansion velocities

Figure 8 shows the radial and core velocities for the expansion of blocks on cylinders and ladders. We note that, while v_c and v_r are nearly independent of J_y/J_x in the range $J_y/J_x = 0.6, \ldots, 1$ for the $L_y = 4$ cylinder [Figs. 8(a),(b)], the values $r_c(t)$ and $\tilde{R}(t)$ themselves actually do decrease when J_y/J_x is tuned from 0.6 to 1 (see Figs. 12 and 13 in Appendix), due to different short-time dynamics. Further, for the accessible times ($t_m = 3\,J_x^{-1}$ for $L_y = 4$), the density profile outside the original block is still completely equivalent to the domain-wall melting. Nevertheless, $r_c(t)$, by definition, is also sensitive to the maximum value in the center of the block, and $\tilde{R}(t)$ is sensitive to the densities at all positions. Thus, the velocities shown in Fig. 8 contain valuable and complementary information.

The two-leg ladder (for which the expansion velocity has been studied in Ref. [70]) shows a behavior similar to the experimental data for 2D expansions [19], namely that the core velocity v_c drops down to zero with increasing J_y/J_x. However, by comparing different L_y, we find a trend towards a faster expansion when L_y is increased at fixed J_y/J_x. This trend is in contrast to the naive expectation that wider cylinders should mimic the 1D-to-2D crossover better. In other words, it demonstrates that the two-leg ladder does not capture all the relevant physics of the expansion in all directions in the 1D-to-2D crossover, although it shows the same qualitative dependence of velocities on J_y/J_x as the 2D system studied experimentally [19]. However, we understand this from our considerations of the limit $J_y \gg J_x$ in Sec. VI C: On the $L_y = 4$ cylinder and the $L_y = 3$ ladder, there exist $E_y = 0$ modes, and thus a preferred occupation of these propagating modes with nonzero k_y is possible. Moreover, in those other cases in which there are no modes with strictly $E_y = 0$, there are at least modes with lower $|E_y| < J_y$.

E. Momentum distribution function

The momentum distribution n_{k_x,k_y} on cylinders starting from $6 \times L_y$ blocks and at fixed time $t = 2.0\,J_x^{-1}$ is shown in Fig. 9. At small $J_y/J_x = 0.2$, we observe a bunching of particles at the $k_x = \pm\frac{\pi}{2a}$ modes independent of k_y, similar to the fully 2D expansion at the same value of J_y/J_x shown in Fig. 4.

For $J_y = J_x$ and on the $L_y = 3$ cylinder, the energy $E_y(k_y = \pm\frac{2\pi}{3a}) = J_y$ can be compensated by kinetic energy $E_x = -2J_x \cos(k_x a)$ in x-direction, compare Eq. (8). Indeed, we find a bunching of particles at those momenta in Fig. 9(e). The $E_y(k_y = 0) = -2J_y$

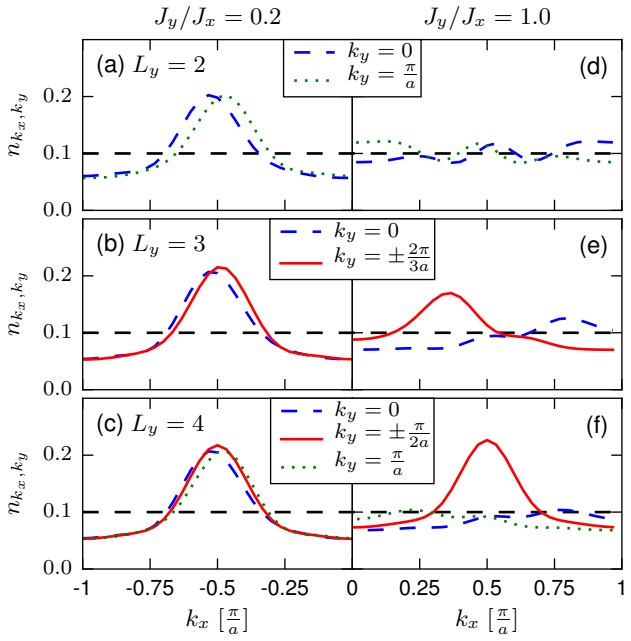

FIG. 9. (Color online) Momentum distribution function n_{k_x,k_y} [dimensionless] for cylinders with (a),(d) $L_y = 2$, (b),(e) $L_y = 3$ and (c),(f) $L_y = 4$, starting from a $6 \times L_y$ cluster. Data are shown for time $t = 2.0\,J_x^{-1}$ and (a)-(c) $J_y/J_x = 0.2$ and (e)-(f) $J_y/J_x = 1.0$ (Note that we have a symmetry $n_{-k_x,k_y} = n_{k_x,k_y} = n_{k_x,-k_y}$). The black dashed lines indicate the flat initial distribution at $t = 0$.

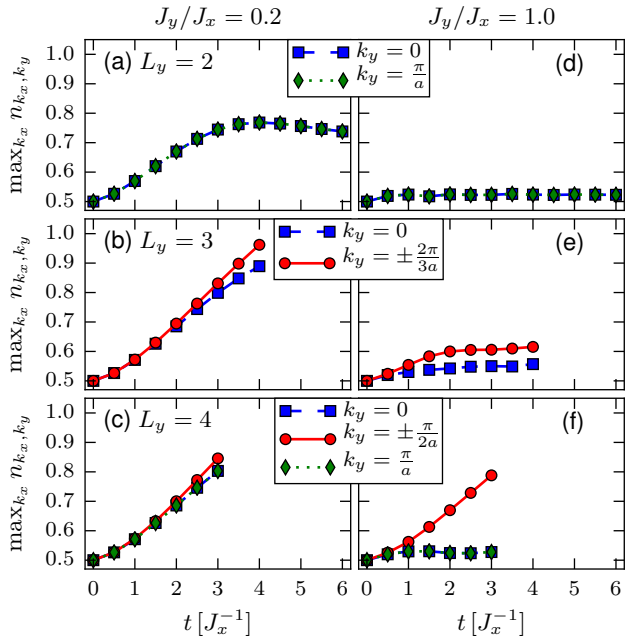

FIG. 10. (Color online) Time evolution of the peak heights in the momentum distribution function for cylinders with (a),(d) $L_y = 2$, (b),(e) $L_y = 3$ and (c),(f) $L_y = 4$, starting from a domain wall. Data are shown for (a)-(c) $J_y/J_x = 0.2$ and (e)-(f) $J_y/J_x = 1.0$.

and $E_y(k_y = \frac{\pi}{a}) = 2J_y$ mode would yield $k_x = \frac{\pi}{a}$ and $k_y = 0$, yet we find a slightly higher weight at smaller k_x in Fig. 9(e). However, we note that all these peaks for $J_y = J_x$ in Figs. 9(d) and (e) are not as high as their counterparts for $J_y/J_x = 0.2$. As we have discussed above and in Appendix B, there are no modes with $E_y = 0$ for $L_y = 2, 3$ on cylinders, hence the maxima in n_{k_x,k_y} are generally suppressed as we go from small to large J_y/J_x for $L_y = 2, 3$.

On the $L_y = 4$ cylinder, we find a bunching of particles at $(k_x, k_y) = (\frac{\pi}{2a}, \frac{\pi}{2a})$ with roughly the same weight for all J_y, compare Figs. 9(c) and (f). This is in agreement with our considerations of Sec. VI C, since the modes with $k_y = \frac{\pi}{2a}$ have $E_y = 0$. The $k_y = 0, \frac{\pi}{a}$ modes are suppressed, similar to the case of $L_y = 2, 3$.

The question of whether the bunching of particles at certain quasimomenta (that requires the existence of propagating modes with energies compatible with those quasimomenta) will lead to a true dynamical quasicondensation at finite momenta can best be addressed using the domain walls as initial stats. Here, we are guided by the behavior of 1D hard-core bosons: In the sudden expansion [70, 80], the dynamical quasicondensation is a transient phenomenon, hence the occupation at $k = \pm\frac{\pi}{2a}$ first increases and then slowly decreases as dynamical fermionization sets in [70, 85, 86]. The crossover between these two regimes – the formation and the decay of quasicondensates – is given by $t_2 \propto B$ (see also the discussion in [16]). For the domain-wall melting, the quasicondensates are continuously fed with particles with identical properties due to the presence of an infinite reservoir and thus the quasicondensation peaks in n_k never decay but keep increasing.

Figure 10 shows the time dependence of the occupation at the maximum of n_{k_x,k_y} for the domain-wall melting on $L_y = 2, 3, 4$ cylinders for (a)-(c) $J_y/J_x = 0.2$ and (d)-(f) $J_y/J_x = 1$. For $J_y/J_x = 0.2$ and the accessible time windows of the $L_y = 3, 4$ cylinders, the occupation indeed increases monotonically in time. On the $L_y = 2$ cylinder in Fig. 10(a), the maximum initially increases similar as for $L_y = 3, 4$, yet for times $t \gtrsim 3J_x^{-1}$ it saturates and even decreases, which suggests that no condensation sets in. Note that the time scale at which the saturation happens is quite large, as it is set by J_y^{-1}. This suggests that there is no condensation even for very small $J_y > 0$ on the $L_y = 2$ cylinder.

The behavior for $J_y/J_x = 1$ is quite different. In almost all cases, the occupation at the maximum quickly saturates, which suggests that no condensation sets in. This observation is consistent with the absence of fast propagating modes on the $L_y = 2, 3$ cylinders. Among the data sets shown in Fig. 10(d)-(f), there is one exception, namely the peak at $(k_x, k_y) = (\frac{\pi}{2a}, \pm\frac{\pi}{2a})$ on the four-leg cylinder, which monotonically increases without a trend towards saturation. This case is thus the most promising candidate for a condensation at $J_y = J_x$.

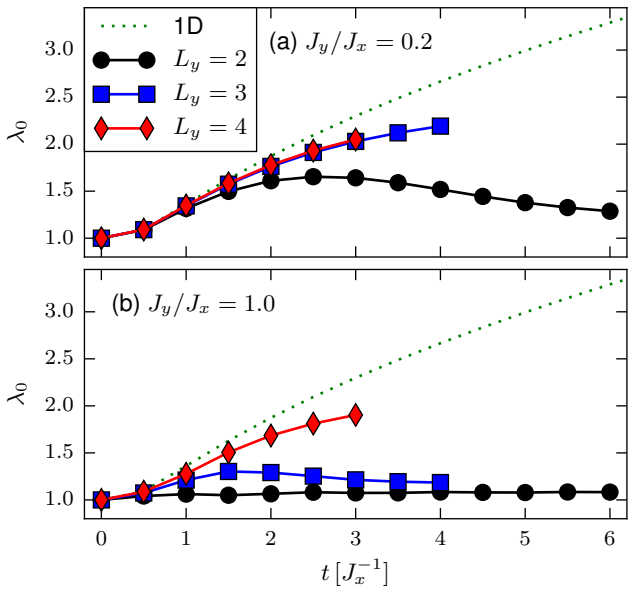

FIG. 11. (Color online) Time evolution of the occupation of the largest eigenvalue λ_0 [dimensionless] of the one particle density matrix for cylinders with (a) $J_y/J_x = 0.2$ and (b) $J_y/J_x = 1.0$, starting from a domain wall. The dotted green line shows the results of an 1D chain ($J_y = 0$) for comparison.

F. Occupation of lowest natural orbital

To investigate the question of condensation in more detail, we look at the maximum occupation λ_0 of the natural orbitals [99]. The natural orbitals are effective single particle states defined as the eigenstates of the one particle density matrix $\langle \hat{a}_\mathbf{i}\, \hat{a}_\mathbf{j} \rangle$. The corresponding eigenvalues sum up to the number of particles and can be interpreted as the occupations of the natural orbitals. A true condensate requires that λ_0 becomes macroscopically large.

The largest occupation λ_0 for the domain-wall melting of cylinders is shown in Fig. 11. In the 1D case, indicated by the green dotted line, the occupation grows, for large times, as $\lambda_0 \approx 1.38\sqrt{t}$ [80]. For $L_y = 2$ we find two degenerate natural orbitals with occupation λ_0. For $J_y/J_x = 0.2$, we find an initial growth for all $L_y = 2, 3, 4$, but for $L_y = 2$, the occupation saturates and even decreases for large times $t \gtrsim 3J_x^{-1}$, similar as for the peaks in the momentum distribution function. In fact, the peaks in the momentum distribution are directly related to the natural orbitals with the largest occupation: For $L_y = 2$ there are two degenerate natural orbitals with maximal occupation with $k_y = 0$ and $k_y = \frac{\pi}{a}$, and their Fourier transformation is peaked slightly above (below) $k_x = \frac{\pi}{2a}$ for $k_y = 0$ ($k_y = \frac{\pi}{a}$). Similarly, for $L_y = 3$ ($L_y = 4$) there are two natural orbitals with maximal occupation with $k_y = \pm\frac{2\pi}{3a}$ ($k_y = \pm\frac{\pi}{2a}$) and one (two) with slightly lower occupation with $k_y = 0$ ($k_y = 0, \frac{\pi}{a}$), leading to the peak structure of Figs. 9(b) and (c) (with peaks only at $k_x > 0$ for domain wall initial states).

For $J_y = J_x$, shown in Fig. 11(b), λ_0 saturates and even decreases for the cylinders of width $L_y = 2, 3$, but keeps growing monotonically for $L_y = 4$ (at least on the time scale accessible to us), in accordance with Figs. 9(f) and 10(f). For $L_y = 4$, we find only two (degenerate) natural orbitals with $k_y = \pm\frac{\pi}{2a}$ with peaks at $k_x = \frac{\pi}{2a}$. Yet, the maximal occupation λ_0 is significantly smaller than in the 1D case and seems to saturate at larger times.

It is instructive to compare λ_0 to the number of particles in the expanding cloud ΔN shown in Fig. 7, defining a condensate fraction $\lambda_0/\Delta N$. ΔN increases linearly in time in 1D, hence the condensate fraction goes to zero with $1/\sqrt{t}$, consistent with the absence of true long range order. In the case of cylinders, we never observe a saturation of $\lambda_0/\Delta N$ to a constant nonzero value, but it keeps decreasing as a function of time. Therefore, a true condensation is not supported by the existing data on all cylinders. Yet, the survival of a quasicondensation on the cylinders is consistent with our data.

VII. SUMMARY

Motivated by recent experiments with ultracold bosons in an optical lattice [16, 19], we simulated the sudden expansion of up to 4×4 hard-core bosons in a 2D lattice. In the limit $J_x \gg J_y$, we find a fast expansion (at least on the timescale accessible to us), similar to the 1D case. When J_y is tuned to the isotropic limit $J_x = J_y$, some fraction of the particles remains as a high-density core in the center and a spherically symmetric shape emerges. This trend is compatible with the observations made in the experiment of Ref. [19]. Unfortunately, our results for the 2D expansion are dominated by surface effects due to the small boson numbers as in fact, in our simulations we have more particles at the boundary of the initial block than in the bulk. This prevents us from analyzing the core expansion velocity [19], yet the radial velocities $v_{r,x}$ decrease monotonically with the block size B at any fixed J_y/J_x. We observe a bunching in the momentum distribution function at quasimomenta compatible with energy conservation. This bunching could signal a dynamical condensation at finite quasimomenta as in the 1D case, where this dynamical quasicondensation [80] has recently been observed in an experiment [16]. Although we cannot ultimately clarify the question of dynamical condensation in 2D with our small clusters, we believe that the bunching of particles at certain finite momenta in the 2D expansion $J_y \approx J_x$ stems from surface effects.

In order to investigate the dimensional crossover further, we studied the expansion on long cylinders and ladders with up to $L_y = 4$ legs. Correlations between the particles in different legs, which lead to a J_y dependence, built up on a very short timescale of about one tunneling time in the longitudinal x-direction. Until a time t_2 that is proportional to the linear dimension of the initial block, the expansion of blocks, restricted to either the left or right half of the system, is identical to the domain-wall

melting. On two-leg ladders, the density in the central region becomes very weakly time dependent and almost stationary for $J_y/J_x \gtrsim 1$, even for the domain walls. This is reflected by a vanishing or even slightly negative core velocity, similar to the observations made in experiments [17, 19]. By considering the limit $J_y \gg J_x$, we argue that this suppressed expansion on the two-leg ladder for large J_y/J_x stems from the fact that there are no modes with $E_y = 0$ on single rungs. For cylinders and ladders with larger $L_y \in \{3, 4\}$, we generically find a faster expansion with higher velocities than in the $L_y = 2$ case. Additionally, there is a dependence of expansion velocities on the boundary conditions in y-direction. For instance, the expansion on $L_y = 4$ cylinder is faster than on a four-leg ladder. In agreement with our considerations of the limit $J_y \gg J_x$, this is accompanied by a bunching at preferred momenta $k_y = \pm\frac{\pi}{2a}$ and $k_x = \pm\frac{\pi}{2a}$ and increasing occupation of natural orbitals. This scenario does not prove the existence of dynamical condensation since the particles in propagating modes will still interact during the expansion, yet identifies the $L_y = 4$ cylinder as a promising candidate system for future studies.

Finally, we state the interesting question whether the expansion velocities on cylinders or ladders will ever show the same dependence on J_y/J_x as the width L_y increases compared to the expansion of a 2D block. The obvious difference is that we fill the cylinders and ladders completely in the y-direction. Due to symmetry, the expansion on cylinders is restricted to be along the x-direction and as such closer to the 1D case, at least for small L_y. There can thus be two scenarios: either, even for $L_y \to \infty$, the velocities of the cylinders might well be above the experimental results or, as L_y increases beyond $L_y = 4$, the velocities at a fixed J_y/J_x will depend non-monotonically on L_y.

Further insight into these questions, i.e., the dependence on L_y or the question of dynamical condensation at finite momenta in dimensions higher than one, could be gained from future experiments with access to measuring the radius. This could be accomplished using single-site resolution techniques, see [100–102] for work in this direction.

Acknowledgments. We acknowledge useful discussions with I. Bloch, L. Pollet, M. Rigol, U. Schneider, and L. Vidmar. F.H.-M. was supported by DFG (Deutsche Forschungsgemeinschaft) Research Unit FOR 1807 through grant no. HE 5242/3-1. Furthermore, we are indebted to M. Rigol for valuable comments on a previous version of the manuscript. This work was also supported in part by National Science Foundation Grant No. PHYS-1066293 and the hospitality of the Aspen Center for Physics.

Appendix A: Extraction of core and radial velocity

Both velocities $v_r = \frac{\partial \tilde{R}(t)}{\partial t}$ and $v_c = \frac{\partial r_c(t)}{\partial t}$ are time derivatives of quantities which are not strictly linear in time. Thus, both v_r and v_c themselves are time dependent. Figure 12 shows the time dependence of the reduced radius $\tilde{R}(t)$, while Fig. 13 shows the core radius $r_c(t)$. In the ideal case we would expect them to get constant in the long-time limit. Unfortunately, our calculations are limited to finite times $t_m = 6\,J_x^{-1}$ for the two-leg ladder, $t_m \approx 4\,J_x^{-1}$ for $L_y = 3$ cylinders/ladders, $t_m \approx 3\,J_x^{-1}$ for $L_y = 4$ cylinders/ladders, and just $t_m \approx 1.5\,J_x^{-1}$ for the 2D lattice.

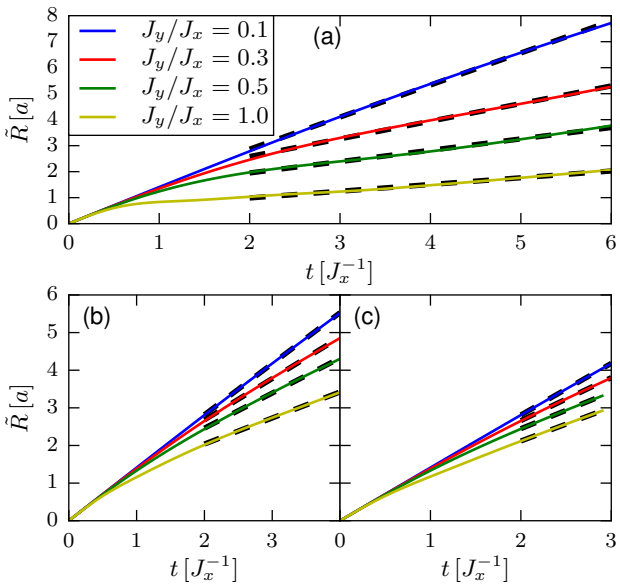

FIG. 12. (Color online) Reduced radius $\tilde{R}(t)$ for cylinders with (a) $L_y = 2$, (b) $L_y = 3$, and (c) $L_y = 4$, starting from a $6 \times L_y$ cluster. The thick dashed lines show the linear fits used to extract the radial velocities v_r, which are shown in Fig. 8(b).

The reduced radii all start as $\tilde{R}(t) = \sqrt{2}tJ_x a$ on very short time scales $t \lesssim 0.5\,J_x^{-1}$. This is clear as we are initially confined to the hopping in x-direction, independently of J_y. For very small $J_y \ll J_x$, the reduced radius remains linear in time with the velocity $v_r = \sqrt{2}J_x a$ at all times, as expected for a ballistic expansion from an initial state with a flat quasimomentum distribution function [19, 92]. A J_y-dependence may show up on a timescale $t \propto J_y^{-1}$. For larger J_y the slope v_r reduces at intermediate times (in the time range where we can observe it) but increases again for large tJ_x. The latter can be understood as follows: the outermost parts have the strongest contribution to the sum in Eq. (3), and naturally these outer parts have the highest velocity $2\,J_x a$ (and also reached a low density such that they are dilute and thus do not see each other any more). Assuming a fraction p of the particles to expand with v and the rest $(1-p)$ to form an inert time-independent block in the center (see also the argument given in [75]), a straightforward calculation shows that $\tilde{R}(t) \approx \sqrt{p}\,v\,t$ at large times. This is also the reason why $\tilde{R}(t)$ does *not* settle to a constant value on the two-leg ladder even

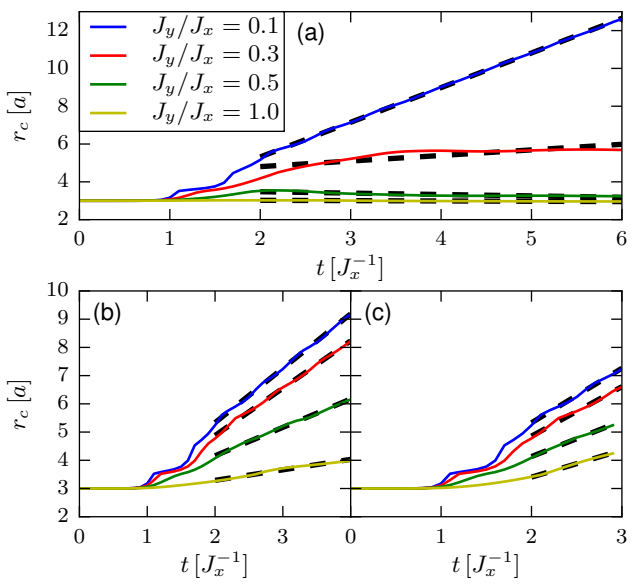

FIG. 13. (Color online) Core radius $r_c(t)$ for cylinders with (a) $L_y = 2$, (b) $L_y = 3$, and (c) $L_y = 4$, starting from a $6 \times L_y$ cluster. The thick dashed lines show the linear fits used to extract the core velocities v_c, which are shown in Fig. 8(a).

for large J_y, although the core in the center barely melts and ΔN becomes only weakly time-dependent: there is always a nonzero fraction of particles which go out from the center.

We extract the time-independent expansion velocities v_r shown in Fig. 3 and 8 by a linear fit $R(t) = v_r \cdot t + \text{const}$ in the time interval $2.0\,J_x^{-1} \leq t \leq t_m$, where t_m is the maximum time reached in the simulations, see the above. For the 2D lattice, we reach only $t_m = 1.5\,J_x^{-1}$, thus we fit only in the interval $1.0\,J_x^{-1} \leq t \leq 1.5\,J_x^{-1}$ in this case. In Fig. 8 we show error bars resulting from similar fits but using only the first or the second half of the time interval.

In the time regime $0 < t < t_2$, the core radius is constant, although the cloud already expands: from both edges, the block melts, but the location of the half-maximum density does not move due to particle-hole symmetry. Just when the first holes arrive in the center of the block, the global maximum decreases and r_c, the half-width-at-half-maximum, begins to increase. It then exhibits strong initial oscillations. The latter stem, on the one hand, from the discreteness of the particles' coordinates on the lattice, which is only partly cured by the linear splines used to extract r_c. On the other hand, the melting of domain walls in one dimension happens in quantized "charges", which lead to well-defined structures in the density profile [96, 103, 104]. Those oscillations prevent us from extracting the core velocity for the 2D lattice, where they are too strong at the times reached in the simulations. Yet, it seems reasonable to extract v_c for the cylinders and ladders by linear fits $r_c(t) = v_c \cdot t + \text{const}$ in the same way as for v_r. While it works quite well for the ballistic expansion at $J_y \ll J_x$ and quite large $J_y \gtrsim J_x$, $r_c(t)$ still exhibits a stronger time dependence for intermediate J_y, e.g., $J_y \approx 0.3 J_x$ on the $L_y = 2$ cylinder. In the latter case, some of the bosons expand initially during the domain-wall melting and thus the block and r_c grow, yet then the expansion is slowed down and the extension of the high-density block measured by r_c becomes weakly time dependent.

Appendix B: Limit of large $J_y \gg J_x$

We split the Hamiltonian (1) into two parts according to $H = \sum_{i_x}(H^y_{i_x} + H^x_{i_x,i_x+1})$, where $H^y_{i_x} = -J_y \sum_{i_y}(\hat{a}^\dagger_{i_x,i_y}\hat{a}_{i_x,i_y+1} + h.c.)$ collects the hopping terms within the rung i_x and $H^x_{i_x,i_x+1}$ collects the hopping terms between neighboring rungs.

1. Two-leg ladder

In the following we give an explicit expression for $H^x_{i_x,i_x+1}$ on a two-leg ladder in terms of the eigenstates of $H^y_{i_x}$ and $H^y_{i_x+1}$. We denote the four eigenstates of $H^y_{i_x}$ on rung i_x as

$$|0\rangle = |\text{vac}\rangle\,, \qquad |1^+\rangle = \frac{\hat{a}^\dagger_{i_x,1} + \hat{a}^\dagger_{i_x,2}}{\sqrt{2}}\,|\text{vac}\rangle\,,$$
$$|2\rangle = \hat{a}^\dagger_{i_x,2}\hat{a}^\dagger_{i_x,1}\,|\text{vac}\rangle\,, \quad |1^-\rangle = \frac{\hat{a}^\dagger_{i_x,1} - \hat{a}^\dagger_{i_x,2}}{\sqrt{2}}\,|\text{vac}\rangle\,, \quad \text{(A1)}$$

where $|\text{vac}\rangle$ denotes the vacuum on rung i_x. The corresponding eigenenergies E_y of $H^y_{i_x}$ are listed in Tab. A1. We then express $\hat{a}_{i_x,i_y}$ and $\hat{a}^\dagger_{i_x,i_y}$ in terms of these eigenstates, plug them into $H^x_{i_x,i_x+1}$ and obtain:

$$\begin{aligned} -H^x_{i_x,i_x+1}/J_x = {} & |0;1^+\rangle\langle 1^+;0| + |0;1^-\rangle\langle 1^-;0| \\ & + |2;1^+\rangle\langle 1^+;2| + |2;1^-\rangle\langle 1^-;2| \\ & + |1^+;1^+\rangle\langle 0;2| - |1^-;1^-\rangle\langle 0;2| \\ & + |1^+;1^+\rangle\langle 2;0| - |1^-;1^-\rangle\langle 2;0| \\ & + h.c.\,. \end{aligned} \quad \text{(A2)}$$

Here, $|\alpha;\beta\rangle \equiv |\alpha\rangle \otimes |\beta\rangle$ with $\alpha, \beta \in \{0, 1^+, 1^-, 2\}$ denotes the tensorproduct of the eigenstates on rungs i_x and $i_x + 1$. The terms in the first two lines of Eq. (A2) correspond to just an exchange of the eigenstates $\alpha \leftrightarrow \beta$ between the neighboring sites. Thus we can identify the terms of the first line to drive the propagation of single bosons on top of the vacuum. The second line can be seen as the propagation of a particle on top of a one-particle background, or alternatively, a single hole in the background of filled rungs.

In contrast to the terms of the first two lines, the terms in the third and fourth row of Eq. (A2) mix different eigenstates. If we imagine to start from a domain wall

$L_y = 2$ ladder			
N	$k_y\,[\frac{\pi}{a}]$	$E_y\,[J_y]$	state
0	0	0	$\|0\rangle$
1	0	-1	$\|1^+\rangle$
	1	1	$\|1^-\rangle$
2	0	0	$\|2\rangle$

$L_y = 4$ cylinder		
N	$k_y\,[\frac{\pi}{a}]$	$E_y\,[J_y]$
0; 4	0	0
1; 3	0	-2
	0.5	0
	-0.5	0
	1	2
2	0	-2.828
	0.5	0
	-0.5	0
	1	0
	1	0
	0	2.828

$L_y = 4$ ladder	
N	$E_y\,[J_y]$
0; 4	0
1; 3	-1.618
	-0.618
	0.618
	1.618
2	-2.236
	-1
	0
	0
	1
	2.236

TABLE A1. Eigenenergies of a single rung. For a given particle number, degenerate levels are listed by their multiplicity.

$|\ldots;2;2;0;0;\ldots\rangle$, those are the terms which "create" the single particle modes $|1^\pm\rangle$ at the border of the domain wall. Subsequently, we would imagine these modes to propagate away to the left as single-hole modes and to the right as single-boson modes. Yet, for the two-leg ladder all these mixing terms change the total energy E_y from 0 to either $+2J_y$ or $-2J_y$. Thus, the creation is only possible via higher-order processes, which are suppressed with increasing J_y/J_x. A term such as $|1^+;1^-\rangle\langle 2;0|$ would not change the total energy E_y, but such a term is not present in Eq. (A2) due to the conservation of total momentum k_y: it would change from $k_y = 0+0$ to $k_y = 0+\frac{\pi}{a}$.

To summarize, we argue that the $L_y = 2$ ladder is special as it possesses the two extremal modes $k_y = 0$ and π with a large energy $E_y = \pm J_y$ for one particle on a rung. We argue that it is not the propagation of the modes $|1^\pm\rangle$ into the vacuum but the creation at the edge of the initial blocks or a domain wall that is suppressed by energy conservation for large $J_y \gg J_x$. As a consequence the current decays very rapidly as evidenced in Fig. 7(a).

2. Larger cylinders and ladders

We turn now to the cylinder and the ladder with $L_y = 4$. The eigenenergies of $H^y_{i_x}$ on a single rung are listed in Tab. A1. Giving an explicit expression for $H^x_{i_x,i_x+1}$ on an $L_y = 4$ cylinder or ladder is not possible here, since it contains too many terms. Nevertheless, we examine its structure. Similar as for the two-leg ladder, we can distinguish between terms which just exchange the eigenstates of neighboring rungs and terms which mix them. As on the two-leg ladder, we associate the exchange terms with the propagation of modes. Since H^x contains only single-particle hopping, the exchange terms appear only between eigenstates with N and $N+1$ bosons on neighboring rungs. Thus, to first order in J_x/J_y, a mode of N bosons can propagate "freely" only in a background of $N\pm 1$ bosons per rung. By definition, all these exchange terms do not change the total energy E_y.

For the mixing terms, there is no restriction on the initial particle numbers on the neighboring rungs. However, $H^x_{i_x,i_x+1}$ obviously preserves the total number of particle, thus there are only mixing terms for $|\ldots N, N'\ldots\rangle \leftrightarrow |\ldots N\pm 1; N'\mp 1\ldots\rangle$. The initial melting of the edge thus happens via a cascade of subsequent mixing processes. For example, consider

$$|\ldots 4;4;0;0\ldots\rangle \to |\ldots 4;3;1;0\ldots\rangle \to |\ldots 4;2;2;0\ldots\rangle \to |\ldots 3;3;2;0\ldots\rangle \to |\ldots 3;3;1;1\ldots\rangle\ . \quad \text{(A3)}$$

On the cylinder there are states with $E_y = 0$ for any number of bosons per rung (see Tab. A1). This makes it plausible that cascades like (A3) are possible without changing E_y on the single rungs. Indeed, we find the corresponding terms in the expression for $H^x_{i_x,i_x+1}$ (not given here). The initial edge of a block or domain wall can thus gradually melt into states with one particle per rung while preserving the energy E_y. This is confirmed by a strong peak in the momentum distribution function depicted in Fig. 9(f). These additional $k_y = \pm\frac{\pi}{2a}$ modes with $E_y = 0$, which are not present in the two-leg ladder, explain thus the trend of a faster expansion seen as higher velocities in Fig. 8. Moreover, we stress that this process is independent of J_y, provided that other modes with $E_y \neq 0$ are suppressed and our picture is applicable. Indeed, we find that the velocities in Fig. 8 and currents (slopes) in Fig. 7(b) are roughly independent of J_y/J_x, even for moderate $J_y/J_x \gtrsim 0.6$.

On the other hand, on the four-leg ladder, there are no states with $E_y = 0$ for one or three bosons on a rung. It is thus immediately clear that there can be no mixing terms which preserve E_y on every rung separately. Moreover, we find that there are also no mixing terms which create modes with opposite energy starting from $E_y = 0$ on both rungs. As a consequence, the domain wall melting on the four-leg ladder requires higher-order processes, similar to the two-leg ladder. However, the necessary intermediate energies $E_y = \pm 0.613 \times 2J_y$ are smaller than for the two-leg ladder, such that these higher-order processes processes are more likely. This is reflected in Fig. 8 by higher velocities for the four-leg ladder compared to the two-leg ladder.

[1] I. Bloch, J. Dalibard, and W. Zwerger, Rev. Mod. Phys. **80**, 885 (2008).

[2] T. Langen, R. Geiger, and J. Schmiedmayer, Annual Rev. of Condensed Matt. Phys. **6**, 201 (2015).

[3] C. Gogolin and J. Eisert, (2015), arXiv:1503.07538 [quant-ph].

[4] J. Eisert, M. Friesdorf, and C. Gogolin, Nature Phys. **11**, 124 (2015).
[5] M. Greiner, O. Mandel, T. Hänsch, and I. Bloch, Nature (London) **419**, 51 (2002).
[6] T. Kinoshita, T. Wenger, and S. D. Weiss, Nature (London) **440**, 900 (2006).
[7] S. Hofferberth, I. Lesanovsky, B. Fisher, T. Schumm, and J. Schmiedmayer, Nature (London) **449**, 324 (2007).
[8] S. Trotzky, Y.-A. Chen, A. Flesch, I. P. McCulloch, U. Schollwöck, J. Eisert, and I. Bloch, Nature Phys. **8**, 325 (2012).
[9] M. Gring, M. Kuhnert, T. Langen, T. Kitagawa, B. Rauer, M. Schreitl, I. Mazets, D. A. Smith, E. Demler, and J. Schmiedmayer, Science **337**, 6100 (2012).
[10] M. Cheneau, P. Barmettler, D. Poletti, M. Endres, P. Schauß, T. Fukuhara, C. Gross, I. Bloch, C. Kollath, and S. Kuhr, Nature (London) **481**, 484 (2012).
[11] D. Pertot, A. Sheikhan, E. Cocchi, L. A. Miller, J. E. Bohn, M. Koschorreck, M. Köhl, and C. Kollath, Phys. Rev. Lett. **113**, 170403 (2014).
[12] S. Will, D. Iyer, and M. Rigol, Nature Communications **6**, 6009 (2015).
[13] S. Braun, M. Friesdorf, S. S. Hodgman, M. Schreiber, J. P. Ronzheimer, A. Riera, M. del Rey, I. Bloch, J. Eisert, and U. Schneider, Proceedings of the National Academy of Sciences **112**, 3641 (2015).
[14] T. Langen, S. Erne, R. Geiger, B. Rauer, T. Schweigler, M. Kuhnert, W. Rohringer, I. E. Mazets, T. Gasenzer, and J. Schmiedmayer, Science **348**, 207 (2015).
[15] L. Xia, L. A. Zundel, J. Carrasquilla, A. Reinhard, J. M. Wilson, M. Rigol, and D. S. Weiss, Nature Phys. **11**, 316 (2014).
[16] L. Vidmar, J. P. Ronzheimer, M. Schreiber, S. Braun, S. S. Hodgman, S. Langer, F. Heidrich-Meisner, I. Bloch, and U. Schneider, Phys. Rev. Lett. **115**, 175301 (2015).
[17] U. Schneider, L. Hackermüller, J. P. Ronzheimer, S. Will, S. Braun, T. Best, I. Bloch, E. Demler, S. Mandt, D. Rasch, and A. Rosch, Nature Phys. **8**, 213 (2012).
[18] A. Reinhard, J.-F. Riou, L. A. Zundel, D. S. Weiss, S. Li, A. M. Rey, and R. Hipolito, Phys. Rev. Lett. **110**, 033001 (2013).
[19] J. P. Ronzheimer, M. Schreiber, S. Braun, S. S. Hodgman, S. Langer, I. P. McCulloch, F. Heidrich-Meisner, I. Bloch, and U. Schneider, Phys. Rev. Lett. **110**, 205301 (2013).
[20] S. Hild, T. Fukuhara, P. Schauß, J. Zeiher, M. Knap, E. Demler, I. Bloch, and C. Gross, Phys. Rev. Lett. **113**, 147205 (2014).
[21] T. Giamarchi, *Quantum Physics in One Dimension* (Clarendon Press, Oxford, 2004) p. 2905.
[22] F. Essler, H. Frahm, F. Göhmann, A. Klümper, and V. E. Korepin, *The one-dimensional Hubbard model* (Cambridge University Press, 2005).
[23] S. R. White, Phys. Rev. Lett. **69**, 2863 (1992).
[24] U. Schollwöck, Rev. Mod. Phys. **77**, 259 (2005).
[25] U. Schollwöck, Ann. Phys. (NY) **326**, 96 (2011).
[26] M. Rigol, V. Dunjko, and M. Olshanii, Nature (London) **452**, 854 (2008).
[27] M. Mierzejewski, L. Vidmar, J. Bonča, and P. Prelovšek, Phys. Rev. Lett. **106**, 196401 (2011).
[28] J. Bonca, M. Mierzejewski, and L. Vidmar, Phys. Rev. Lett. **109**, 156404 (2012).
[29] G. S. Uhrig, Phys. Rev. A **80**, 061602 (2009).
[30] S. A. Hamerla and G. S. Uhrig, Phys. Rev. B **89**, 104301 (2014).
[31] F. Goth and F. F. Assaad, Phys. Rev. B **85**, 085129 (2012).
[32] G. Carleo, F. Becca, M. Schiró, and M. Fabrizio, Sci. Rep. **2**, 243 (2012).
[33] G. Carleo, F. Becca, L. Sanchez-Palencia, S. Sorella, and M. Fabrizio, Phys. Rev. A **89**, 031602 (2014).
[34] E. Gull, A. J. Millis, A. I. Lichtenstein, A. N. Rubtsov, M. Troyer, and P. Werner, Rev. Mod. Phys. **83**, 349 (2011).
[35] M. Eckstein, A. Hackl, S. Kehrein, M. Kollar, M. Moeckel, P. Werner, and F. A. Wolf, Eur. Phys. J. Special Topics **180**, 217 (2010).
[36] M. Moeckel and S. Kehrein, Phys. Rev. Lett. **100**, 175702 (2008).
[37] F. Queisser, K. V. Krutitsky, P. Navez, and R. Schützhold, Phys. Rev. A **89**, 033616 (2014).
[38] J. Lux, J. Müller, A. Mitra, and A. Rosch, Phys. Rev. A **89**, 053608 (2014).
[39] J. Lux and A. Rosch, Phys. Rev. A **91**, 023617 (2015).
[40] R. Schützhold, M. Uhlmann, Y. Xu, and U. R. Fischer, Phys. Rev. Lett. **97**, 200601 (2006).
[41] M. Schiró and M. Fabrizio, Phys. Rev. Lett. **105**, 076401 (2010).
[42] M. Schiró and M. Fabrizio, Phys. Rev. B **83**, 165105 (2011).
[43] M. Jreissaty, J. Carrasquilla, F. A. Wolf, and M. Rigol, Phys. Rev. A **84**, 043610 (2011).
[44] A. Jreissaty, J. Carrasquilla, and M. Rigol, Phys. Rev. A **88**, 031606(R) (2013).
[45] N. Schlünzen, S. Hermanns, M. Bonitz, and C. Verdozzi, (2015), arXiv:1503.07538 [cond-mat.quant-gas].
[46] S. Yan, D. A. Huse, and S. R. White, Science **332**, 1173 (2011).
[47] S. Depenbrock, I. P. McCulloch, and U. Schollwöck, Phys. Rev. Lett. **109**, 067201 (2012).
[48] E. Stoudenmire and S. R. White, Annual Review of Condensed Matter Physics **3**, 111 (2012).
[49] N. Maeshima, Y. Hieida, Y. Akutsu, T. Nishino, and K. Okunishi, Phys. Rev. E **64**, 016705 (2001).
[50] F. Verstraete and J. Cirac, (2004), arXiv:cond-mat/0407066.
[51] J. Jordan, R. Orús, G. Vidal, F. Verstraete, and J. I. Cirac, Phys. Rev. Lett. **101**, 250602 (2008).
[52] P. Corboz, S. R. White, G. Vidal, and M. Troyer, Phys. Rev. B **84**, 041108 (2011).
[53] M. P. Zaletel, R. S. K. Mong, C. Karrasch, J. E. Moore, and F. Pollmann, Phys. Rev. B **91**, 165112 (2015).
[54] J. J. Dorando, J. Hachmann, and G. K.-L. Chan, The Journal of Chemical Physics **130**, 184111 (2009).
[55] J. Haegeman, J. I. Cirac, T. J. Osborne, I. Pižorn, H. Verschelde, and F. Verstraete, Phys. Rev. Lett. **107**, 070601 (2011).
[56] M. Lubasch, V. Murg, U. Schneider, J. I. Cirac, and M.-C. Bañuls, Phys. Rev. Lett. **107**, 165301 (2011).
[57] A. J. A. James and R. M. Konik, Phys. Rev. B **92**, 161111 (2015).
[58] G. Vidal, Phys. Rev. Lett. **93**, 040502 (2004).
[59] A. Daley, C. Kollath, U. Schollwöck, and G. Vidal, J. Stat. Mech.: Theory Exp. (2004), P04005.
[60] S. R. White and A. E. Feiguin, Phys. Rev. Lett. **93**,

076401 (2004).
[61] R. C. Brown, R. Wyllie, S. B. Koller, E. A. Goldschmidt, M. Foss-Feig, and J. V. Porto, Science **348**, 540 (2015).
[62] T. Antal, Z. Rácz, A. Rákos, and G. M. Schütz, Phys. Rev. E **57**, 5184 (1998).
[63] D. Gobert, C. Kollath, U. Schollwöck, and G. Schütz, Phys. Rev. E **71**, 036102 (2005).
[64] J. Lancaster and A. Mitra, Phys. Rev. E **81**, 061134 (2010).
[65] J. Caux and J. Mossel, J. Stat. Mech. (2011), P02023.
[66] L. F. Santos and A. Mitra, Phys. Rev. E **84**, 016206 (2011).
[67] T. Sabetta and G. Misguich, Phys. Rev. B **88**, 245114 (2013).
[68] J. C. Halimeh, A. Wöllert, I. P. McCulloch, U. Schollwöck, and T. Barthel, Phys. Rev. A **89**, 063603 (2014).
[69] V. Alba and F. Heidrich-Meisner, Phys. Rev. B **90**, 075144 (2014).
[70] L. Vidmar, S. Langer, I. P. McCulloch, U. Schneider, U. Schollwöck, and F. Heidrich-Meisner, Phys. Rev. B **88**, 235117 (2013).
[71] R. Steinigeweg, F. Heidrich-Meisner, J. Gemmer, K. Michielsen, and H. De Raedt, Phys. Rev. B **90**, 094417 (2014).
[72] C. Karrasch, D. M. Kennes, and F. Heidrich-Meisner, Phys. Rev. B **91**, 115130 (2015).
[73] D. Muth, D. Petrosyan, and M. Fleischhauer, Phys. Rev. A **85**, 013615 (2012).
[74] C. D. E. Boschi, E. Ercolessi, L. Ferrari, P. Naldesi, F. Ortolani, and L. Taddia, Phys. Rev. A **90**, 043606 (2014).
[75] S. Sorg, L. Vidmar, L. Pollet, and F. Heidrich-Meisner, Phys. Rev. A **90**, 033606 (2014).
[76] F. Heidrich-Meisner, S. R. Manmana, M. Rigol, A. Muramatsu, A. E. Feiguin, and E. Dagotto, Phys. Rev. A **80**, 041603 (2009).
[77] J. Kajala, F. Massel, and P. Törmä, Phys. Rev. Lett. **106**, 206401 (2011).
[78] J. Schönmeier-Kromer and L. Pollet, Phys. Rev. A **89**, 023605 (2014).
[79] I. Hen and M. Rigol, Phys. Rev. Lett. **105**, 180401 (2010).
[80] M. Rigol and A. Muramatsu, Phys. Rev. Lett. **93**, 230404 (2004).
[81] M. Rigol and A. Muramatsu, Mod. Phys. Lett. B **19**, 861 (2005).
[82] A. Micheli, A. J. Daley, D. Jaksch, and P. Zoller, Phys. Rev. Lett. **93**, 140408 (2004).
[83] A. J. Daley, S. R. Clark, D. Jaksch, and P. Zoller, Phys. Rev. A **72**, 043618 (2005).
[84] K. Rodriguez, S. Manmana, M. Rigol, R. Noack, and A. Muramatsu, New J. Phys. **8**, 169 (2006).
[85] M. Rigol and A. Muramatsu, Phys. Rev. Lett. **94**, 240403 (2005).
[86] A. Minguzzi and D. M. Gangardt, Phys. Rev. Lett. **94**, 240404 (2005).
[87] S. Fölling, S. Trotzky, P. Cheinet, M. Feld, R. Saers, A. Widera, T. Müller, and I. Bloch., Nature (London) **448**, 1029 (2007).
[88] A. Celi, P. Massignan, J. Ruseckas, N. Goldman, I. B. Spielman, G. Juzeliūnas, and M. Lewenstein, Phys. Rev. Lett. **112**, 043001 (2014).
[89] B. K. Stuhl, H.-I. Lu, L. M. Aycock, D. Genkina, and I. B. Spielman, Science **349**, 1514 (2015).
[90] M. Mancini, G. Pagano, G. Cappellini, L. Livi, M. Rider, J. Catani, C. Sias, P. Zoller, M. Inguscio, M. Dalmonte, and L. Fallani, (2015), arXiv:1502.02495 [cond-mat.quant-gas].
[91] M. A. Cazalilla, R. Citro, T. Giamarchi, E. Orignac, and M. Rigol, Rev. Mod. Phys. **83**, 1405 (2011).
[92] S. Langer, M. J. A. Schuetz, I. P. McCulloch, U. Schollwöck, and F. Heidrich-Meisner, Phys. Rev. A **85**, 043618 (2012).
[93] D. Jukić, B. Klajn, and H. Buljan, Phys. Rev. A **79**, 033612 (2009).
[94] Z. Mei, L. Vidmar, F. Heidrich-Meisner, and C. Bolech, , in preparation (unpublished).
[95] F. Verstraete, D. Porras, and J. I. Cirac, Phys. Rev. Lett. **93**, 227205 (2004).
[96] D. Gobert, C. Kollath, U. Schollwöck, and G. Schütz, Phys. Rev. E **71**, 036102 (2005).
[97] A. Trombettoni and A. Smerzi, Phys. Rev. Lett. **86**, 2353 (2001).
[98] H. Hennig, T. Neff, and R. Fleischmann, (2013), arXiv:1309.7939 [nlin.PS].
[99] O. Penrose and L. Onsager, Phys. Rev. **104**, 576 (1956).
[100] P. M. Preiss, R. Ma, M. E. Tai, A. Lukin, M. Rispoli, P. Zupancic, Y. Lahini, R. Islam, and M. Greiner, Science **347**, 1229 (2015).
[101] T. Fukuhara, A. Kantian, M. Endres, M. Cheneau, P. Schauß, S. Hild, C. Gross, U. Schollwöck, T. Giamarchi, I. Bloch, and S. Kuhr, Nature Phys. **9**, 235 (2013).
[102] T. Fukuhara, P. Schauß, M. Endres, S. Hild, M. Cheneau, I. Bloch, and C. Gross, Nature **506**, 76 (2013).
[103] V. Hunyadi, Z. Rácz, and L. Sasvári, Phys. Rev. E **69**, 066103 (2004).
[104] V. Eisler and Z. Rácz, Phys. Rev. Lett. **110**, 060602 (2013).